



Centrum voor Wiskunde en Informatica

REPORTRAPPORT

Uniqueness conditions in a hyperbolic model for oil recovery
by steamdrive

J. Bruining, C.J. van Duijn

Modelling, Analysis and Simulation (MAS)

MAS-R9803 February 28, 1998

Report MAS-R9803
ISSN 1386-3703

CWI
P.O. Box 94079
1090 GB Amsterdam
The Netherlands

CWI is the National Research Institute for Mathematics and Computer Science. CWI is part of the Stichting Mathematisch Centrum (SMC), the Dutch foundation for promotion of mathematics and computer science and their applications.

SMC is sponsored by the Netherlands Organization for Scientific Research (NWO). CWI is a member of ERCIM, the European Research Consortium for Informatics and Mathematics.

Copyright © Stichting Mathematisch Centrum
P.O. Box 94079, 1090 GB Amsterdam (NL)
Kruislaan 413, 1098 SJ Amsterdam (NL)
Telephone +31 20 592 9333
Telefax +31 20 592 4199

Uniqueness Conditions in a Hyperbolic Model for Oil Recovery by Steamdrive

J. Bruining

Dietz Laboratory, Mijnbouwstraat 120, 2628 RX Delft, The Netherlands

email: `j.bruining@mp.tudelft.nl`

C.J. van Duijn

CWI, P.O. Box 94079, 1090 GB Amsterdam, The Netherlands

email: `hansd@cwil.nl`

ABSTRACT

In this paper we study a one-dimensional model for oil recovery by steamdrive. This model consists of two parts: a (global) interface model and a (local) steam condensation/capillary diffusion model. In the interface model a steam condensation front (SCF) is present as an internal boundary between the hot steam zone (containing water, oil and steam) and the cold liquid zone (containing only water and oil). Disregarding capillary pressure away from the SCF, a 2x2 hyperbolic system arises for the water and steam saturation. This system cannot be solved uniquely without additional conditions at the SCF. To find such conditions we make a blow up of the SCF and consider a parabolic transition model, including capillary diffusion. We study in detail the existence conditions for travelling wave solutions. These conditions translate into the missing matching conditions at the SCF in the hyperbolic limit and thus provide uniqueness. We show that different transition models yield different matching conditions, and thus different solutions of the interface model. We also give a relatively straightforward approximation and investigate its validity for certain ranges of model parameters.

1991 Mathematics Subject Classification: 35L65, 76S05, 76T05.

Keywords and Phrases: Multiphase flow, porous media, hyperbolic system, (non) uniqueness, travelling waves.

Note: Work carried out under project MAS1.3 'Partial Differential Equations in Porous Media Research'.

1 Introduction

Steamdrive, being the most important enhanced oil recovery technique, received considerable attention in the engineering literature during the past decades. As examples we mention the

experimental work of Kimber et al. [10], Gümrah et al. [8] and Farouq Ali et al. [5], and the modeling work of Mandl & Volek [14], Godderij et al. [7] and Prats [18]. An important characteristic of their models is the occurrence of a steam condensation front (SCF) as an internal boundary between the hot steam zone and the cold liquid zone. Furthermore, in their approach the saturation of the oil remaining behind in the steam zone does not follow from an analysis of the models, but is apriori given as model parameter.

A relatively simple model which takes the oil saturation in the steam zone as an unknown into account, was proposed by Shutler [21]. We will explain it in some detail because it forms the basis of our approach. In this model again a SCF is assumed which separates an upstream steam zone from a downstream oil/water zone. Furthermore it is assumed that all steam impinging on the SCF condenses, The velocity of the SCF follows from a local heat balance. Because the heat capacity of the porous medium depends on the fluid saturations, there exists a coupling between the heat balance and the saturation equations. Although the coupling is weak, Shutler takes it into account. Because fluid saturations are constant at the SCF, he finds that its velocity is constant as well. The steam zone is considered as a zone of constant high temperature in which oil and non-condensing gas (steam) are present at connate water saturation. In the downstream cold zone oil and water are present at the original reservoir temperature. Capillary forces are disregarded. Water and oil conservation equations applied at the SCF, combined with the Buckley-Leverett equation for gas/oil in the steam zone and the Buckley-Leverett equation for oil/water in the cold zone, lead to a complete solution of the model equations. However, the assumption that the steam zone contains only connate water is not clear. This assumption is apparently necessary to close the problem. It may also have an undesirable effect on the prediction of the efficiency of the steamdrive process. Models related to the one of Shutler have been proposed by Pope [17] and Yortsos [28].

Recently Wingard & Orr [27] extended the model of Shutler to incorporate three phase flow in the steam zone. Superheated steam was injected leading to three temperature zones: a zone at constant superheated injection temperature with only oil and steam at connate water saturation, a steam zone at boiling temperature with oil, water, and steam and a cold zone with water and oil. It appears that the solution resulting from this model is not unique because there are two more unknowns than equations. Because the solution domain in the phase diagram is rather small, however, a representative solution was found. The work of Wingard and Orr clearly demonstrates that the hyperbolic interface model of steamdrive requires additional conditions if a unique solution is to be obtained. From the physical point of view it is expected that such conditions originate from detailed modeling of the steam condensation process itself. Menegus & Udell [15] have carried out a theoretical analysis and

an experimental study that focusses on steam condensation in porous media, see also Udell [25] and Udell & Fitch [26]. These studies focus on steam-water flow and use a semi-steady state approach. In this paper they play an important role when modeling the transition between the steam zone and the cold liquid zone. We have simplified their models by disregarding capillary effects on the boiling temperature.

In this paper we present a one dimensional model of steamdrive, where oil with no distillable components is displaced by steam and where capillary forces are disregarded away from the SCF. The model includes a submodel for steam condensation in a transition zone. In that submodel, steam condenses according to a delta distribution at the SCF and fluid flow towards and from the SCF is governed by Darcy's law including capillary effects. The model equations in the transition zone are solved by the method of matched asymptotic expansions yielding traveling wave type solutions, where the wave speed equals the speed of the SCF. The conditions for such waves to exist are precisely the missing matching conditions for the saturations at the SCF. We will explicitly show how different transition models yield different saturation combinations at the SCF and consequently different solutions of the hyperbolic model. These differences are not always small. For instance when comparing the results of a transition model with constant capillary diffusion and one with Brooks-Corey three phase capillary pressures, the differences are well-noticeable and cannot be disregarded for practical purposes. But small or not, differences are present and a selection has to be made. Such non-uniqueness is known to occur in systems of conservation laws. This in contrast with a single hyperbolic transport equation. Then the actual form of the regularizing capillary pressure has no effect on the uniqueness in the hyperbolic limit, as long as the regularization yields a parabolic differential equation.

In Section 2 we describe the physical model. First we present the base case, with input parameters summarized in Table I and Table II. In the base case we model the transition region with constant (saturation independent) capillary diffusion, an abrupt temperature drop from steam temperature to reservoir temperature at the SCF and no steam downstream of the SCF. We also present three cases in which one of these simplifying conditions is relaxed (i) Brooks-Corey three-phase capillary pressures, (ii) an exponential temperature decline downstream the SCF, and (iii) a non-zero steam saturation downstream the SCF in the transition region. In Section 3 we present the mathematical formulation of the base case. In Section 4 we show that without a transition model non-uniqueness occurs. We illustrate this by comparing the results of the three cases defined in Section 2 with the base case. Section 5 deals with the practical application of the theory. Here we introduce the average oil saturation in the steam zone and investigate its dependence on reservoir and fluid properties. To construct the full solution of the steamdrive problem is very involved. Therefore we present in Section

5 an easy to find approximation as well. In Figure 13 we compare the results for the full solution and this approximation in terms of the average oil saturation in the steam zone. It clearly indicates in which parameter range the approximation is acceptable. We summarize our findings in Section 6 which contains the conclusions.

We conclude this section with a mathematical remark about the structure of the traveling waves in the transition region. Only when considering ‘viscosity’ solutions according to the base case, which involves the identity matrix to describe the smoothing due to capillary diffusion, we are able to find monotone traveling waves. We conjecture that this monotonicity is closely related to an entropy condition of the type of Liu [13], giving ‘uniqueness’ for the hyperbolic limit. Indeed, when we deviate from the base case to show non-uniqueness, we find in all cases non-monotone waves. To make this precise is beyond the scope of this paper and will be subject to future research. However, one conclusion definitely can be drawn: there does not exist a universal entropy condition for the steamdrive problem, since existence conditions for solutions in the (vanishing) transition region depend on the details of the transition model, and carry over to solutions of the hyperbolic system.

2 Physical model

Oil displacement by steamdrive through a porous medium is a complex physical process which is controlled by the steam condensation process and by viscous and capillary forces, see for instance Wingard & Orr [27] or Stewart & Udell [23]. In this paper we propose a simplified approach in which all steam condenses at an a priori known Steam Condensation Front (SCF) and in which capillary forces as well as temperature variations are disregarded except in a small neighbourhood of that front. Here “small” must be understood in a suitable dimensionless context. To model this we consider a global *interface model* in which capillary forces are absent on any scale and in which the interface (SCF) separates the hot steam zone from the remainder of the reservoir. Further we consider a local *transition model* which takes capillary forces and temperature variations into account at the SCF. The transition model yields the correct matching conditions at the SCF in the hyperbolic interface model.

In modeling a one dimensional flood through a reservoir we consider the porous medium to be homogeneous, with constant porosity ϕ , and of semi-infinite extent. The multiphase flow (oil, water, steam (gas)) through the reservoir is directed in what we choose to be the positive x -axis. Hence the phase saturations S_o , S_w , and S_g are functions of position x and time t only, see Figure 1. Initially, at $t = 0$, the reservoir contains oil and connate water: i.e. for all $x > 0$

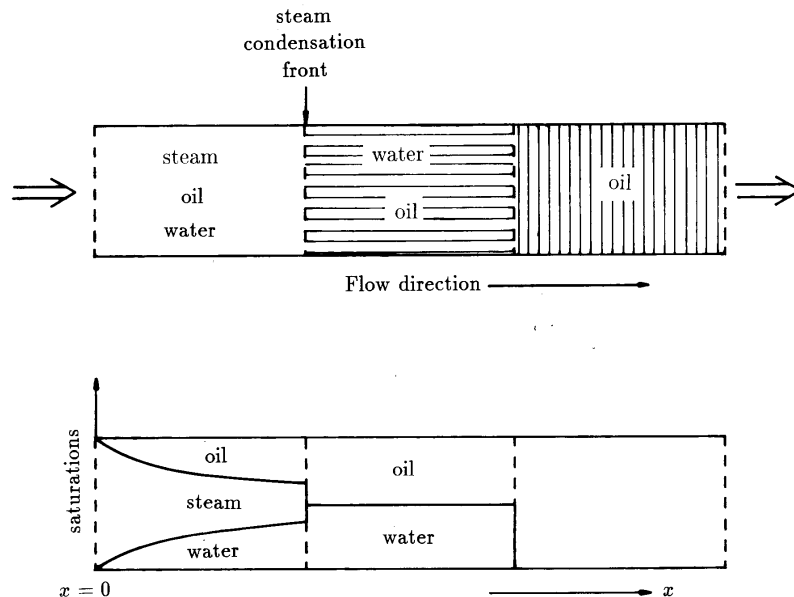


Figure 1: Sketch of the one dimensional steam displacement process and the phase saturations.

$$S_o(x, 0) = 1 - S_{wc} , S_w(x, 0) = S_{wc} , S_g(x, 0) = 0 \quad . \quad (2.1)$$

From the left steam of 100 % quality is injected at rate u_{inj} : i.e at $x = 0$ and for all $t > 0$

$$S_o(0, t) = 0 , S_w(0, t) = S_{wc} , S_g(0, t) = 1 - S_{wc} \quad . \quad (2.2)$$

In writing these initial and boundary conditions we assume that the residual oil and gas saturations are constant. Without loss of generality they are given the value zero: see also Table I, where the values of all quantities used throughout this paper are given.

Oil and water are produced at the right, in our simplified model at $x = \infty$. All fluids, also steam, are considered incompressible. To avoid non-essential complications the thermal expansion coefficients of the fluids are taken to be zero. Heat losses to the surroundings as well as gravity effects are not considered. Furthermore, we assume that the oil is non-distillable i.e. the partial vapour pressure of the oil in the gas phase is negligible. Consequently we ignore the presence of a distillable oil bank.

2.1 Interface model

We distinguish two zones, see Figure 1, one upstream and one downstream relative to the SCF. *Upstream* is the steam zone. We assume that this zone is at constant steam temperature T_1 ,

thus disregarding the temperature gradient as a consequence of the pressure gradient driving the fluids and the boiling point curve. Capillary forces are neglected and fluid transport is governed by Darcy's law for multiphase flow. With the exception of Section 5, we use power law expressions for the relative permeabilities. In this work we keep the exponents fixed and all equal to four, see Table II. Any other choice greater than one would give the same qualitative results. *Downstream* is the liquid zone where only oil and water are present. This zone is at constant reservoir temperature T_o . Again capillary forces are disregarded and fluid transport is governed by Darcy's law for multiphase flow. The relative permeabilities are the same as in the steam zone.

Because oil and water experience different temperatures, their viscosities $\mu_{i=o,w}$ may vary substantially. To account for this we take the well-known expressions, e.g. see Reid et al. [19] and Table I,

$$\ln \frac{\mu_i}{\mu_r} = a_i + \frac{b_i}{T} \quad i = o, w \quad . \quad (2.3)$$

The two zones are separated by the SCF. The velocity of this front v_{st} is determined from a local heat balance, in which the heat released by the condensing steam impinging on the SCF is equal to the amount of heat necessary to warm up the reservoir, see Mandl and Volek [14]. The result is

$$v_{st} = \frac{\rho_g \Delta H u_{inj}}{(\rho c)_r (T_1 - T_o)} \quad , \quad (2.4)$$

The symbols appearing in this expression are explained in Table I. The effective heat capacity of the reservoir includes the heat capacity of the matrix and the fluids in the pores. Variations in saturations have a relatively small effect on the effective heat capacity. This allows us to decouple the balance equations for heat and for mass. Therefore we may consider the velocity of the SCF as a given quantity.

In the interface approach the steam condenses at the SCF, $x = v_{st}t$, only. Due to condensation there occurs water production Q_w [$m^3/(m^3 s)$], i.e. volume of produced water due to condensation per unit volume reservoir and per unit time, according to

$$Q_w = \frac{\rho_g}{\rho_w} r \delta(x - v_{st}t) \quad , \quad (2.5)$$

and steam loss Q_g [$\text{m}^3/(\text{m}^3 \text{ s})$], i.e. the volume of condensed steam per unit volume of reservoir per unit time, according to

$$Q_g = r\delta(x - v_{\text{st}}t) . \quad (2.6)$$

Here $\delta()$ [$1/\text{m}$] denotes the Dirac distribution and r [m/s] the a priori unknown steam condensation rate. This factor has to be determined from the saturations at the SCF. Using the values of the parameters in Table I, we find only a weak dependence of r on the saturations. Computations show that r is almost equal to the steam injection rate, see Section 3.3.

In order to match saturations across the SCF we need to make a detailed analysis of the possible transitions occurring there. For this we need a model which is outlined below.

2.2 Transition model

In the transition model we regularize the (possible) discontinuous saturations at the SCF by incorporating capillary effects. In addition we have to specify the condensation process as well as the temperature variation within the transition region. We shall first formulate a simple base case to illustrate the underlying ideas and then define three extensions.

2.2.1 Base case

Here we assume that the effect of capillary forces can be described in terms of a constant diffusivity D . In Section 3.2 we let $D \downarrow 0$ in the appropriate dimensionless setting (i.e. we let $\frac{D}{Lu_{\text{inj}}} \downarrow 0$), which yields the missing matching conditions at the SCF. When $\frac{D}{Lu_{\text{inj}}}$ is small, we have a small transition region which is centered at the SCF and which travels with the same velocity, see Figure 2. To study the saturations within the transition region we introduce the dimensionless variable

$$\xi = \frac{x - v_{\text{st}}t}{L} \frac{Lu_{\text{inj}}}{D} \quad (2.7)$$

and consider the blow up as $D/Lu_{\text{inj}} \downarrow 0$. In terms of ξ this yields a transition region extending from $\xi = -\infty$ to $\xi = +\infty$. The corresponding limit saturations have the form of traveling waves. As $\xi \rightarrow -\infty$ the waves have to be matched with the outer saturations in the steam (hot) zone and as $\xi \rightarrow +\infty$ with the outer saturations in the liquid (cold) zone.

For simplicity we assume that also in the transition region the steam condenses at the SCF, where $\xi = 0$. Consequently two transition sub-regions can be identified: one upstream and one

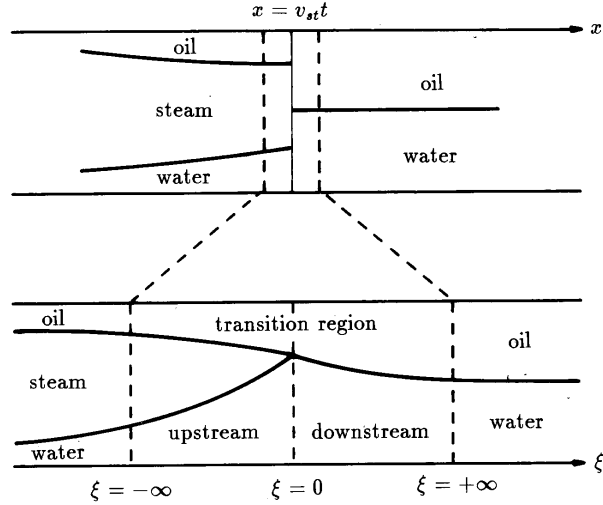


Figure 2: Sketch of transition region between the steam zone and the cold zone. The transition region consists of the SCF, an upstream region with steam of constant temperature and a downstream region. In the base case, the downstream region has the cold reservoir temperature and no steam is present there. Possible extensions are discussed in Sections 2.2.2 - 2.2.4

downstream the SCF. In both sub-regions we assume again that the temperature is constant: i.e.

$$T(\xi) = \begin{cases} T_1 & \text{for } \xi < 0 \quad , \\ T_o & \text{for } \xi > 0 \quad . \end{cases} \quad (2.8)$$

We use this expression in the viscosity formula (2.3) to account for the temperature change in the transition region.

Expression (2.8) implies that the temperature in the downstream zone is below the boiling point temperature. Assuming local thermodynamic equilibrium, this means that no steam can be present there. In particular it implies

$$S_g(0) = 0 \quad . \quad (2.9)$$

It turns out that this condition is needed as well to obtain a unique set of matching conditions at the SCF in the interface model.

2.2.2 Brooks-Corey capillary pressure diffusion

In this extension of the base case we keep (2.8) and (2.9) but we take the capillary forces more realistically into account. Clearly, this involves the introduction of three phase capillary pressures. Since experimental data are hardly available, we assume that the oil-water capillary pressure $p_o - p_w$ only depends on the water saturation and the steam-oil capillary pressure $p_g - p_o$ only on the steam saturation (see e.g. Aziz & Settari [1]). Combining these pressures an expression results for the steam-water capillary pressure $p_g - p_w$. Thus in this approach, three phase capillary pressures can be expressed in terms of well-known two-phase capillary pressures. The saturation dependence of the capillary pressures enters through the Leverett-functions. We write

$$P_c^{\text{ow}} = \sigma \sqrt{\frac{\phi}{k}} J^{\text{ow}}(S_w) \quad \text{and} \quad P_c^{\text{go}} = \sigma \sqrt{\frac{\phi}{k}} J^{\text{go}}(S_g) \quad , \quad (2.10)$$

where we have used the fact that the interfacial tension (σ) between oil and water and between gas and oil is approximately the same. For the Leverett functions we use the empirical Brooks-Corey expressions, see for instance Dullien [4]. This means that J^{ow} is proportional to

$$\left(\frac{S_w - S_{\text{wc}}}{1 - S_{\text{wc}}} \right)^{-1/\lambda_s} \quad , \quad (2.11)$$

where λ_s is a factor related to the sorting. The expression for J^{go} is obtained by substituting $S_w = 1 - S_g$ into (2.11).

When λ_s is large the capillary pressure curve is flat, meaning that the grains have approximately the same size and are well sorted. When λ_s is small the capillary pressure is steep, and the grains are badly sorted. Finally we assume that the Leverett function satisfies $J(\frac{1}{2}) = \frac{1}{2}$. For most experimental data, as in [4], indeed $0.3 < J(\frac{1}{2}) < 0.7$. An analysis based on the Carmen-Kozeny equation for permeability and the surface free energy of the porous medium also shows that $J(\frac{1}{2}) \approx \frac{1}{2}$. All of this leads to an expressions for the capillary pressure of the form

$$P_c^{\text{ow}} = \frac{\sigma}{2} \sqrt{\frac{\phi}{k}} \left(\frac{\frac{1}{2} - S_{\text{wc}}}{1 - S_{\text{wc}}} \right)^{1/\lambda_s} \left(\frac{S_w - S_{\text{wc}}}{1 - S_{\text{wc}}} \right)^{-1/\lambda_s} \quad \text{and} \quad P_c^{\text{go}}(S_g) = P_c^{\text{ow}}(1 - S_g) \quad . \quad (2.12)$$

In writing (2.12) we have disregarded hysteresis effects. One can expect that the drainage curve (non-wetting phase is invading) is somewhat above this curve and that the imbibition curve (wetting phase is invading) is below this curve.

In Section 4 we introduce the capillary pressure functions in the different equations. This leads to terms resembling non-linear diffusion. As a characteristic capillary diffusion number we find

$$D = \frac{\sigma\sqrt{\phi k}}{\mu_o} \quad (2.13)$$

As in the base case we investigate the process $\frac{D}{Lu_{inj}} \downarrow 0$ to obtain matching conditions for the interface model.

2.2.3 Temperature variation

Here we consider constant capillary diffusion and (2.9) but we modify (2.8). To model the temperature distribution properly, one should have to consider the heat-balance equation in terms of the local coordinate ξ and find a solution satisfying $T \rightarrow T_1$ as $\xi \rightarrow -\infty$ and $T \rightarrow T_o$ as $\xi \rightarrow +\infty$. This procedure may be complicated because the coefficients in the temperature equation depend on the fluid saturations. Ignoring this dependence, Miller [16] finds a solution of the form

$$T(\xi) = \begin{cases} T_1 & \text{for } \xi < 0 \\ T_o + (T_1 - T_o)e^{-\alpha\xi} & \text{for } \xi > 0 \end{cases} \quad (2.14)$$

Here the constant α is the ratio of the thermal conductivity and the front velocity in the appropriate dimensionless setting.

2.2.4 Positive steam saturation at SCF

Now we consider a constant capillary diffusivity and (2.8) but we modify (2.9). If we drop the assumption concerning local thermodynamic equilibrium, then there is no physical reason why (2.9) would hold. In that case, steam condenses at a rate which is limited by diffusional processes in the vapor zone. Corresponding to this we construct solutions for which steam is also present in the downstream region. To obtain such solutions we have to prescribe a positive value for the steam saturation at the SCF:

$$S_g(0) > 0 \quad (\text{prescribed}) \quad . \quad (2.15)$$

Remark: In Section 5 we discuss the results of computations for the full Brooks-Corey case. There we keep (2.8) and (2.9) in the transition model, but we modify both the capillary pressure and relative permeabilities according to Brooks-Corey expressions. This is a

modification of Section (2.2.2) in the sense that power law relative permeabilities are replaced by the Brooks-Corey-Stone relative permeabilities, where $k_{rw} = k_{rw}(S_w)$, $k_{rg} = k_{rg}(S_g)$ and $k_{ro} = k_{ro}(S_w, S_g)$.

Table I, Summary of physical input parameters ¹			
<i>Physical quantity</i>	<i>symbol</i>	<i>value</i>	<i>unit</i>
characteristic length	L	100	[m]
steam temperature	T_1	486	[K]
reservoir temperature	T_o	313	[K]
injection rate steam	u_{inj}	$9.52 \cdot 10^{-4}$	[m ³ /m ² /s]
steam viscosity	μ_g	$1.63 \cdot 10^{-5}$	[Pa s]
oil viscosity at T_1	$\mu_o(T_1)$	$2.45 \cdot 10^{-3}$	[Pa s]
oil viscosity at T_o	$\mu_o(T_o)$	0.180	[Pa s]
water viscosity at T_1	$\mu_w(T_1)$	$1.30 \cdot 10^{-4}$	[Pa s]
water viscosity at T_o	$\mu_w(T_o)$	$7.21 \cdot 10^{-4}$	[Pa s]
viscosity $\ln \mu_i/\mu_r = a_i + b_i/T$	μ_i	$\mu_i(T)$	[Pa s]
reference viscosity	μ_r	1	[Pa s]
coefficient in oil viscosity	a_o	-13.79	[-]
coefficient in oil viscosity	b_o	3781	[K]
coefficient in water viscosity	a_w	-12.06	[-]
coefficient in oil viscosity	b_w	1509	[K]
Brooks-Corey sorting factor	λ_s	2	[-]
enthalpy $H_2O(l)(T_o) \rightarrow H_2O(g)(T_1)$	ΔH	2636	[kJ/kg]
effective heat capacity of rock	$(\rho c)_r$	2029	[kJ/m ³ /K]
thermal coefficient in (2.14)	α	0.017	[-]
capillary diffusion constant	D	$2.2 \cdot 10^{-7}$	[m ² /s]
velocity SCF	v_{st}	$7.12 \cdot 10^{-5}$	[m/s]
porosity	ϕ	0.38	[m ³ /m ³]
permeability	k	$4.3 \cdot 10^{-13}$	[m ²]
interfacial tension	σ	$30 \cdot 10^{-3}$	[N/m]
water density	ρ_w	1000	[kg/m ³]
steam density	ρ_g	10.2	[kg/m ³]
connate water saturation	S_{wc}	0.15	[m ³ /m ³]
residual gas saturation	S_{gr}	0.0	[m ³ /m ³]
residual oil saturation	S_{or}	0.0	[m ³ /m ³]

¹The values of the steam parameters in Table I assume a steam pressure of 20 bar. Furthermore the value of the thermal coefficient α is based on a thermal diffusivity of $9.85 \cdot 10^{-7}$ [m²/s]. Note that this coefficient is proportional to the ratio of the capillary and thermal diffusivity.

Table II, Expressions for relative permeabilities		
symbol	quantity	expression
k_{rw}	water permeability	$((S_w - S_{wc})/(1 - S_{wc}))^4$
k_{ro}	oil permeability	$(S_o/(1 - S_{wc}))^4$
k_{rg}	steam permeability	$(S_g/(1 - S_{wc}))^4$

3 Mathematical formulation of base case

3.1 Interface model

The interface model described in Section 2.1 yields the following mass balance equations

$$\phi \frac{\partial S_w}{\partial t} + \frac{\partial u f_w}{\partial x} = Q_w = \frac{\rho_g}{\rho_w} r \delta(x - v_{st} t) \quad , \quad (3.1)$$

$$\phi \frac{\partial S_g}{\partial t} + \frac{\partial u f_g}{\partial x} = -Q_g = -r \delta(x - v_{st} t) \quad , \quad (3.2)$$

$$\phi \frac{\partial S_o}{\partial t} + \frac{\partial u f_o}{\partial x} = 0 \quad . \quad (3.3)$$

The non-zero terms in the right side of equations (3.1) and (3.2) are a consequence of the steam condensation at the SCF, see also expressions (2.5) and (2.6). Except for these terms, system (3.1)-(3.3) consists of the standard multiphase flow equations in which u denotes the total specific discharge and f_i ($i=o,w,g$) the fractional flow functions

$$f_i = \frac{M_{oi} k_{ri}}{M_{ow} k_{rw} + k_{ro} + M_{og} k_{rg}} \quad , \quad (3.4)$$

where M_{oi} are the mobility ratio's

$$M_{oi} = \frac{\mu_o}{\mu_i} \quad . \quad (3.5)$$

Note that these quantities have different values up and downstream the SCF. This is due to the temperature dependence of the viscosity which enters through equations (2.3). In the interface model we will not write this dependence explicitly. Furthermore note that the specific

discharge u and the steam condensation rate r are both unknown and have to be determined from the problem. However, by adding equations (3.1)-(3.3) and using $\sum S_i = \sum f_i = 1$, we find the volume balance

$$\frac{\partial u}{\partial x} = -r\left(1 - \frac{\rho_g}{\rho_w}\right)\delta(x - v_{st}t) \quad .$$

Applying the boundary condition $u(0, t) = u_{inj}$ (steam injection rate), we find upon integration

$$u = u(x, t) = u_{inj} - r\left(1 - \frac{\rho_g}{\rho_w}\right)H(x - v_{st}t) \quad , \quad (3.6)$$

where H denotes the Heaviside function: $H(s) = 0$ for $s < 0$ and $H(s) = 1$ for $s > 0$. Thus the phase saturations and the constant r have to be determined from equations (3.1)-(3.3), (3.6) and the initial-boundary conditions (2.1), (2.2).

Next we rewrite the equations in dimensionless form by redefining

$$\begin{aligned} S_w &:= \frac{S_w - S_{wc}}{1 - S_{wc}}, & S_o &:= \frac{S_o}{1 - S_{wc}}, & S_g &:= \frac{S_g}{1 - S_{wc}} \\ t &:= \frac{u_{inj}t}{\phi L}, & u &:= \frac{u}{u_{inj}}, & x &:= \frac{x}{L} \quad , \end{aligned}$$

and by introducing the dimensionless steam condensation rate

$$\Lambda = \frac{r}{u_{inj}} \quad , \quad (3.7)$$

and the dimensionless SCF velocity

$$v = \frac{v_{st}}{u_{inj}}\phi(1 - S_{wc}) \quad . \quad (3.8)$$

Eliminating the oil saturation by setting $S_o = 1 - S_w - S_g$, we obtain the steamdrive problem (Problem SD): Find the phase saturations S_w , S_g and the condensation constant Λ such that

$$\frac{\partial S_w}{\partial t} + \frac{\partial u f_w}{\partial x} = \frac{\rho_g}{\rho_w}\Lambda\delta(x - vt) \quad , \quad (3.9)$$

$$\frac{\partial S_g}{\partial t} + \frac{\partial u f_g}{\partial x} = -\Lambda\delta(x - vt) \quad , \quad (3.10)$$

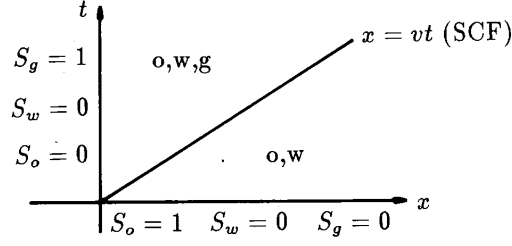


Figure 3: Distribution of phases in the x,t plane

and

$$u = 1 - \Lambda \left(1 - \frac{\rho_g}{\rho_w}\right) H(x - vt) \quad , \quad (3.11)$$

for $x > 0$ and $t > 0$, subject to initial-boundary conditions

$$S_w(x, 0) = 0 \quad , \quad S_g(x, 0) = 0 \quad \text{for all } x > 0 \quad , \quad (3.12)$$

and

$$S_w(0, t) = 0 \quad , \quad S_g(0, t) = 1 \quad \text{for all } t > 0 \quad . \quad (3.13)$$

We shall consider solutions of this problem for which no steam is present in the downstream region: i.e. we pose the additional condition (as part of Problem SD)

$$S_g(x, t) = 0 \quad \text{for } x > vt, t > 0 \quad . \quad (3.14)$$

This seems a natural condition since the temperature in this region is the cold reservoir temperature T_o at which no steam can survive at the current reservoir pressure. In Figure 3 we show the regions in which the various phases are present.

In analyzing Problem SD, we shall frequently represent (part of) the solution as an orbit in the (S_w, S_g) plane (phase plane). Since $0 \leq S_w + S_g = 1 - S_o \leq 1$, this orbit is confined to the closed triangular domain \mathcal{D} in Figure 4. The vertices are denoted by $O = (0,0)$, $T = (0,1)$ and $A(1,0)$. Note that any orbit representing a solution must pass through the points T

(boundary conditions) and O (initial conditions), and must coincide with part of the S_w -axis (solution in the cold zone where $S_g = 0$).

In the steam zone where the three phases are present and where $u = 1$, we have to solve equations (3.9) and (3.10), which we write in vector notation as

$$\frac{\partial \mathbf{S}}{\partial t} + \frac{\partial}{\partial x} \mathbf{f}(\mathbf{S}) = \mathbf{0} \quad , \quad (3.15)$$

in which \mathbf{S} and \mathbf{f} denote the column vectors $\mathbf{S} = (S_w, S_g)^T$ and $\mathbf{f} = (f_w, f_g)^T$. The eigenvalues λ_1 and λ_2 of the Jacobian matrix

$$D\mathbf{f} = \begin{pmatrix} f_{ww} & f_{wg} \\ f_{gw} & f_{gg} \end{pmatrix} \quad , \quad (3.16)$$

where $f_{ij} = \frac{\partial f_i}{\partial S_j}$ ($i, j = w, g$), are given by

$$\lambda_k(\mathbf{S}) = \frac{1}{2}(f_{ww} + f_{gg}) + (-1)^k \sqrt{\{(f_{ww} - f_{gg})^2 + 4f_{wg}f_{gw}\}} \quad . \quad (3.17)$$

We verified computationally that

$$0 \leq \lambda_1 < \lambda_2 \quad \text{in} \quad \mathcal{D} \setminus \{O, A, T\} \quad (3.18)$$

and

$$\lambda_1 = \lambda_2 = 0 \quad \text{at} \quad O, A \quad \text{and} \quad T \quad . \quad (3.19)$$

Thus the system (3.15) is strictly hyperbolic in the triangle \mathcal{D} , except at the vertices which are called umbilic points, see Schaeffer & Shearer [20]. The independent right eigenvectors of $D\mathbf{f}$ are denoted by $\mathbf{t}_k = \mathbf{t}_k(\mathbf{S})$, $k=1,2$. A solution of (3.15), satisfying constant boundary conditions, consists in general of a combination of shock waves, constant states and rarefaction waves, see for example Lax [11], LeVeque [12], Smoller [22], or Hellferich [9]. Rarefaction waves are self-similar solutions depending on $\eta = x/t$ only. Considering $\mathbf{S} = \mathbf{S}(\eta)$, we find from (3.15) that they satisfy

$$-\eta \frac{d\mathbf{S}}{d\eta} + \frac{d}{d\eta} \mathbf{f}(\mathbf{S}) = \mathbf{0} \quad (3.20)$$

or

$$-\eta \frac{d\mathbf{S}}{d\eta} + D\mathbf{f} \frac{d\mathbf{S}}{d\eta} = 0 \quad . \quad (3.21)$$

in which we recognize an eigenvalue problem for the matrix $D\mathbf{f}$. Hence

$$\frac{d\mathbf{S}}{d\eta} = \alpha(\eta) \mathbf{t}_k(\mathbf{S}) \quad (3.22)$$

and

$$\eta = \lambda_k(\mathbf{S}) \quad , \quad (3.23)$$

where α is an η -dependent proportionality factor which is a priori unknown. As a consequence of (3.23) we observe that a rarefaction wave is only possible if along its orbit in the phase plane the eigenvalue varies monotonically. Differentiating (3.23) with respect to η and using (3.22) gives

$$1 = \nabla \lambda_k(\mathbf{S}) \cdot \frac{d\mathbf{S}}{d\eta} = \alpha(\eta) \nabla \lambda_k(\mathbf{S}) \cdot \mathbf{t}_k(\mathbf{S}) \quad , \quad (3.24)$$

where ∇ denotes the gradient in the phase plane. Substituting this into (3.22) yields the system

$$\frac{d\mathbf{S}}{d\eta} = \frac{1}{\nabla \lambda_k(\mathbf{S}) \cdot \mathbf{t}_k(\mathbf{S})} \mathbf{t}_k(\mathbf{S}) \quad , \quad (3.25)$$

as long as $\nabla \lambda_k(\mathbf{S}) \cdot \mathbf{t}_k(\mathbf{S}) \neq \mathbf{0}$ (genuine nonlinearity, Lax [11]).

If a rarefaction is to be part of the solution of Problem SD we obviously want

$$\lambda_2(\mathbf{S}) \leq v \quad , \quad (3.26)$$

since otherwise the rarefaction would exceed the SCF, yielding a multivalued solution. The region where (3.26) holds strictly is indicated in Figure 4 as the set \mathcal{D}_l above the curve

$$l = \{(S_w, S_g) : \lambda_2(S_w, S_g) = v\} \quad . \quad (3.27)$$

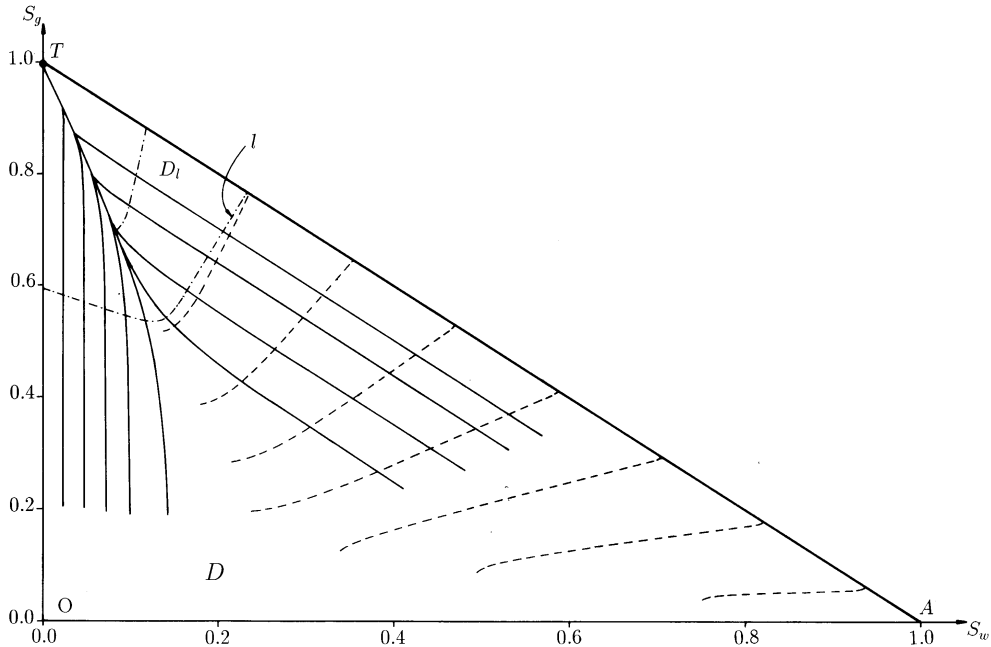


Figure 4: Slow (dashed) and fast (solid) rarefactions, see (3.25)

In spite of (3.26) we computed solutions of the system (3.25) in the full triangular domain \mathcal{D} . Though not strictly necessary for the analysis presented here, this gives a complete picture of the slow and fast rarefaction waves in the phase-plane. For $k=2$, the fast rarefactions, we solved (3.25) for $\eta < v$ and for $\eta > v$ with initial values $(S_w(v), S_g(v)) \in l$. Computing the orbits backwards in η we found that they all reached the top T , i.e. the boundary conditions, at $\eta = 0$: see Figure 4 where several of these fast rarefactions are shown (solid curves). The degenerate behavior of the right side of equations (3.25) causes the collapse of the orbits in the top of the triangle. This is discussed in detail by Schaeffer & Shearer [20].

For $k=1$, the slow rarefactions, we solved (3.25) forwards in η with initial values taken from the segment AT . The corresponding start value of η is

$$\eta = \lambda_1(S_w, S_g) \quad \text{with} \quad (S_w, S_g) \in AT \quad (3.28)$$

These slow rarefactions are also shown in Figure 4 (dashed curves). Both slow and fast rarefactions are shown up to points where the eigenvalues reach a local extremum (along the corresponding orbits).

We will not discuss the occurrence of shocks in the steam zone because they do not arise for

our choice of boundary conditions. To find a solution of Problem SD we will use only fast rarefactions or constant states upstream the SCF. Later on in Section 3.3 where we discuss the matching conditions at the SCF, we show in fact that constant states are not allowed. Thus the solution for $x < vt$ consists of a fast rarefaction only.

If a pair $(S_w^*, S_g^*) \in \text{AT}$ represents a boundary condition different from (3.13), then the corresponding solution in the steam zone starts with a slow rarefaction (since $\lambda_1(S_w^*, S_g^*) = 0$), followed by a constant state, then followed by a fast rarefaction to match up with the SCF. This can only occur for boundary conditions above the line l provided the ensuing slow rarefaction does not intersect l before transition to the fast path.

Next we turn to the cold region downstream the SCF. Because of (3.14), only oil and water are present there. Hence we are left with the two phase Buckley-Leverett equation

$$\frac{\partial S_w}{\partial t} + u^+ \frac{\partial f_w}{\partial x} = 0 \quad \text{for } x > vt, t > 0, \quad (3.29)$$

where u^+ denotes the downstream velocity, see (3.11),

$$u^+ = 1 - \Lambda \left(1 - \frac{\rho_g}{\rho_w}\right) \quad . \quad (3.30)$$

We need to solve equation (3.29) with the apriori unknown saturation $S_w^+ := \lim_{x \downarrow vt} S_w(x, t)$ along the SCF and with $S_w = 0$ initially. Assuming S_w^+ to be constant and using standard Buckley-Leverett (hyperbolic) theory, we find that the entropy solutions consist of shocks or rarefactions followed by shocks. Furthermore, only if the speed of the rarefactions or the shocks exceeds the speed of the SCF we find non-trivial solutions. With reference to Figure 5 this implies that

$$S_* \leq S_w^+ \leq S^* \quad (\text{non-trivial solutions}), \quad (3.31)$$

where S_* is the (smallest) root of

$$f_w(S_w)/S_w = v/u^+ \quad (3.32)$$

and S^* is the largest root of

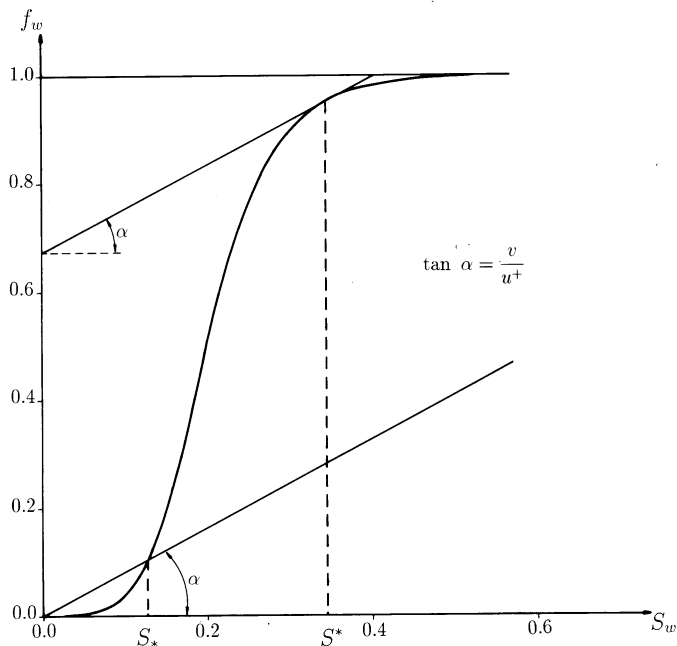


Figure 5: Construction of admissible S_w^+ interval

$$\frac{df_w(S_w)}{dS_w} = v/u^+, \quad (3.33)$$

or

$$S_w^+ = 0 \quad (\text{trivial solution}) \quad . \quad (3.34)$$

The value S_* corresponds to the smallest shock possible with speed $\geq v$, and S^* corresponds to the largest rarefaction possible with speed $\geq v$.

To match the conditions across the SCF we need to consider the local behavior at the SCF by means of the transition model. We shall use the notation

$$S_i^{+(-)} = \lim_{x \downarrow (\uparrow) vt} S_i(x, t) \quad i = g, w \quad . \quad (3.35)$$

As a consequence of (3.14) we have $S_g^+ = 0$

3.2 Transition Model

In the transition model we include capillary forces in the form of a constant diffusivity D in all three balance equations (3.1)-(3.3). To recast the equations in dimensionless form we proceed as in the previous section. Introducing in addition the dimensionless diffusivity

$$\varepsilon = \frac{D}{u_{\text{inj}}L} \quad , \quad (3.36)$$

we obtain for the water and steam saturations

$$\frac{\partial S_w}{\partial t} + \frac{\partial u f_w}{\partial x} = \frac{\rho_g}{\rho_w} \Lambda \delta(x - vt) + \varepsilon \frac{\partial^2 S_w}{\partial x^2} \quad , \quad (3.37)$$

$$\frac{\partial S_g}{\partial t} + \frac{\partial u f_g}{\partial x} = -\Lambda \delta(x - vt) + \varepsilon \frac{\partial^2 S_g}{\partial x^2} \quad , \quad (3.38)$$

where again u and Λ satisfy (3.11). Here ε is a small number which will be considered to converge towards zero. Using the values from Table I we find as a typical value $\varepsilon = 2.34 \cdot 10^{-6}$. Next consider the stretched moving coordinate (see also (2.7))

$$\xi = \frac{x - vt}{\varepsilon} \quad (3.39)$$

Regarding S_w and S_g as functions of ξ and t , we find instead of (3.37 and 3.38) the equations

$$\varepsilon \frac{\partial S_w}{\partial t} - v \frac{\partial S_w}{\partial \xi} + \frac{\partial u f_w}{\partial \xi} = \frac{\rho_g}{\rho_w} \Lambda \delta(\xi) + \frac{\partial^2 S_w}{\partial \xi^2} \quad , \quad (3.40)$$

$$\varepsilon \frac{\partial S_g}{\partial t} - v \frac{\partial S_g}{\partial \xi} + \frac{\partial u f_g}{\partial \xi} = -\Lambda \delta(\xi) + \frac{\partial^2 S_g}{\partial \xi^2} \quad . \quad (3.41)$$

For ε small, in fact letting $\varepsilon \downarrow 0$, we find to leading order

$$S_i(\xi, t) = S_i(\xi) \quad i = w, g \quad , \quad (3.42)$$

where the traveling wave type transition saturations satisfy

$$-v \frac{\partial S_w}{\partial \xi} + \frac{\partial u f_w}{\partial \xi} = \frac{\rho_g}{\rho_w} \Lambda \delta(\xi) + \frac{\partial^2 S_w}{\partial \xi^2} \quad , \quad (3.43)$$

$$-v \frac{\partial S_g}{\partial \xi} + \frac{\partial u f_g}{\partial \xi} = -\Lambda \delta(\xi) + \frac{\partial^2 S_g}{\partial \xi^2} \quad , \quad (3.44)$$

for $-\infty < \xi < \infty$. These equations imply

$$-vS_w + uf_w = \frac{\rho_g}{\rho_w} \Lambda H(\xi) + \frac{dS_w}{d\xi} + C_1 \quad , \quad (3.45)$$

$$-vS_g + uf_g = -\Lambda H(\xi) + \frac{dS_g}{d\xi} + C_2 \quad , \quad (3.46)$$

where C_1 and C_2 are constants of integration. Because the base case temperature satisfies (2.8), we find that the water and oil viscosity and hence the mobility ratios M_{ow} and M_{og} have different values for $\xi > 0$ and $\xi < 0$. This means that the fractional flow functions in equations (3.45) and (3.46) also have a discontinuous ξ -dependence: $f_i = f_i^r(S_w, S_g)$ for $\xi > 0$ and $f_i = f_i^l(S_w, S_g)$ for $\xi < 0$.

We solve the transition saturation equations subject to the boundary conditions (3.35):

$$S_w(-\infty) = S_w^- \quad , \quad S_g(-\infty) = S_g^- \quad (3.47)$$

and

$$S_w(+\infty) = S_w^+ \quad , \quad S_g(+\infty) = 0 \quad . \quad (3.48)$$

Letting $\xi \rightarrow \pm\infty$ in (3.45) and (3.46) yields the Rankine-Hugoniot condition

$$\text{RH} \begin{cases} u^+ f_w^+ - vS_w^+ & = \frac{\rho_g}{\rho_w} \Lambda + f_w^- - vS_w^- \\ 0 & = -\Lambda + f_g^- - vS_g^- \end{cases} \quad , \quad (3.49)$$

where $f_i^- = f_i^l(S_w^-, S_g^-)$ and $f_w^+ = f_w^r(S_w^+, S_g^+)$.

We will formulate conditions, in addition to (3.26), (3.31) and (3.49), which enable us to select a unique set of boundary values (3.47), (3.48). These conditions are related to the solvability of the boundary value problem (3.45)-(3.48). To investigate this we consider two sub-problems. Eliminating the constants C_1 and C_2 from equations (3.45) and (3.46), we consider for $\xi < 0$ the boundary value problem

$$P^l \begin{cases} \frac{dS_w}{d\xi} & = f_w^l - vS_w - (f_w^- - vS_w^-) \\ \frac{dS_g}{d\xi} & = f_g^l - vS_g - (f_g^- - vS_g^-) \\ S_w(-\infty) & = S_w^- \quad , S_w(0) = S_w^l \\ S_g(-\infty) & = S_g^- \quad , S_g(0) = S_g^l \end{cases} \quad (3.50)$$

and for $\xi > 0$

$$P^r \left\{ \begin{array}{l} \frac{dS_w}{d\xi} = u^+ f_w^r - v S_w - (u^+ f_w^+ - v S_w^+) \\ \frac{dS_g}{d\xi} = u^+ f_g^r - v S_g \\ S_w(+\infty) = S_w^+ , S_w(0) = S_w^r \\ S_g(+\infty) = 0 , S_g(0) = S_g^r \end{array} \right. \quad (3.51)$$

where we have used that $u^+ f_g^+ - v S_g^+ = 0$. We need to find such boundary values S_w^- , S_g^- and S_w^+ , so that the subproblems P^l and P^r admit a solution with $S_w^l = S_w^r$ and $S_g^l = S_g^r$. For that choice we have continuous transition saturations that satisfy equations (3.45) and (3.46). Only if we make the additional assumption (2.9) about the value of the steam saturation at the SCF, we find unique values S_w^- , S_g^- and S_w^+ . This will be explained in the next section.

3.3 Matching Conditions

We first consider Problem P^l . To determine the nature of the equilibrium point (S_w^-, S_g^-) we compute the eigenvalues e_k ($k=1,2$) of the linearized system at that point. This yields

$$e_k = \lambda_k - v \quad , \quad (3.52)$$

where λ_k are the eigenvalues of the Jacobian matrix $D\mathbf{f}$, see (3.17). Consequently, if we take $(S_w^-, S_g^-) \in \mathcal{D}_l$, we find that $e_1 < e_2 < 0$. This means that no non-trivial orbit is possible that ends up in (S_w^-, S_g^-) as $\xi \rightarrow -\infty$. Combining this information with (3.26) we find as remaining possibility $(S_w^-, S_g^-) \in l$: in other words, the saturations at the upstream side of the SCF must satisfy the condition

$$\lambda_2(S_w^-, S_g^-) = v \quad , \quad (3.53)$$

implying that (S_w^-, S_g^-) is a saddle with $e_1 < e_2 = 0$. Given a pair (S_w^-, S_g^-) satisfying this condition, we find the orbit that represents the solution of Problem P^l by the following shooting procedure. Let $S_g(0)$ be the prescribed value of the steam saturation at the SCF. We fix $S_g^l = S_g(0)$ in Problem P^l and take S_w^l as a shooting parameter: that is we solve the equations in Problem P^l by a fourth order Runge Kutta procedure in negative ξ -direction with

start values (S_w^l, S_g^l) . The corresponding orbit will deflect either to the left or to the right, see Figure 6 (top). Applying the bisection method, one finds after a number of iterations an extremely accurate approximation of the water saturation at the origin $S_w(0) = S_w^l$ for which a solution exists at the given values of S_w^-, S_g^- and $S_g(0)$.

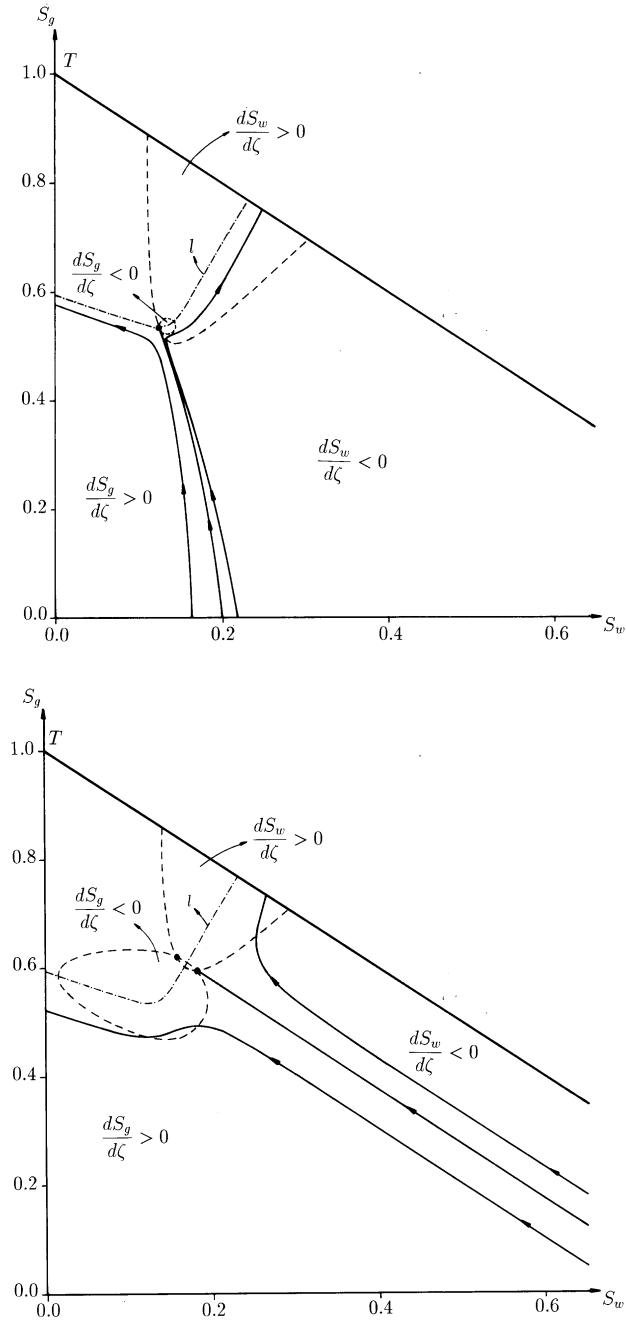


Figure 6: Shooting procedure to solve Problem P^1 . Here $S_g(0) = 0$ Top: flow diagram for $(S_w^-, S_g^-) \in l$. Bottom: flow diagram for $(S_w^-, S_g^-) \in \mathcal{D}_l$. The dots indicate the location of equilibrium points. The orbits are pointing in negative ξ direction and $\zeta = -\xi$.

At this point it is instructive to consider the dynamics of solutions in the saturation triangle more closely. Because we solve the equations in the negative ξ -direction, we put

$$\zeta = -\xi \quad (3.54)$$

and consider the initial value problem

$$\begin{cases} \frac{dS_w}{d\zeta} &= (f_w^- - vS_w^-) - f_w^l + vS_w \quad , \\ \frac{dS_g}{d\zeta} &= (f_g^- - vS_g^-) - f_g^l + vS_g \quad , \\ S_w(0) &= S_w^l, S_g(0) = S_g^l \quad . \end{cases} \quad (3.55)$$

The qualitative behavior of orbits is determined by the location of equilibrium points and curves where either $\frac{dS_w}{d\zeta} = 0$ or $\frac{dS_g}{d\zeta} = 0$. This is shown in Figure 6 for two locations of (S_w^-, S_g^-) . In the top figure we have chosen $(S_w^-, S_g^-) \in l$. The location of the curves where either $\frac{dS_w}{d\zeta} = 0$ or $\frac{dS_g}{d\zeta} = 0$ suggests the existence of only one equilibrium point being (S_w^-, S_g^-) . Three orbits are shown in this figure, all originating from the base line $S_g = 0$: one deflects to the left and one deflects to the right of the equilibrium. The middle orbit approximates the solution that reaches (S_w^-, S_g^-) as $\zeta \rightarrow \infty$. In the bottom figure we have chosen $(S_w^-, S_g^-) \in \mathcal{D}_l$. The location of the separation curves now suggests the existence of two equilibria: one inside \mathcal{D}_l , being the chosen (S_w^-, S_g^-) and one outside \mathcal{D}_l . Observe from the sign conditions that no orbit can reach (S_w^-, S_g^-) as $\zeta \rightarrow \infty$. This corresponds to the earlier observation about the negative sign of the eigenvalues of the linearized system near that point.

Let us now introduce the additional hypothesis (2.9), expressing that also in the transition zone the steam saturation vanishes at the SCF:

$$S_g(0) = S_g^l = S_g^r = 0 \quad (3.56)$$

Using this assumption we propose the following procedure for Problem P^l . Choose S_w^- , find the corresponding S_g^- so that (3.53) holds and apply the above described shooting procedure with (3.56) to find the water saturation at the SCF. This yields S_w^l as a function of S_w^- . With the values taken from Table I, we computed this function and the result is shown in Figure 7.

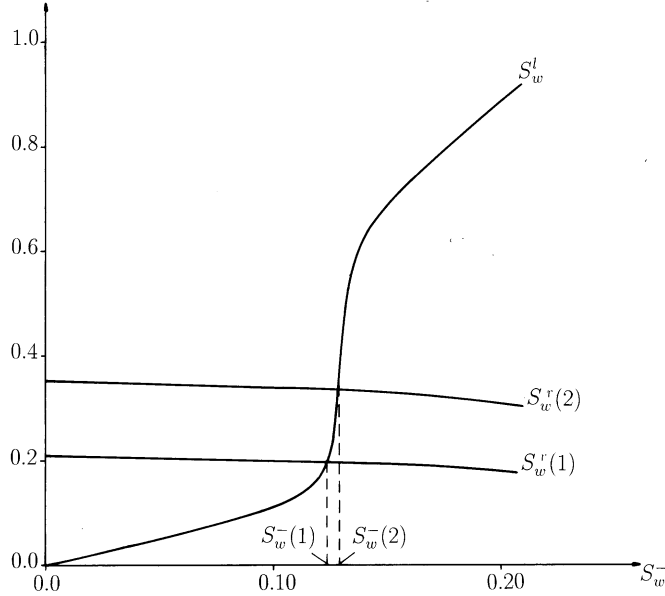


Figure 7: Water saturation at the SCF as a function of S_w^- . The curve $S_w^r(1)$ is computed with the base case temperature (2.8) in the transition zone. The curve $S_w^r(2)$ is computed with the temperature (2.14) in the transition zone.

Note that S_w^l depends continuously and monotonically on S_w^- and that $S_w^l = 0$ whenever $S_w^- = 0$.

Next we consider Problem P^r . First note, by eliminating the constant Λ from the Rankine-Hugoniot conditions (3.49) and using condition (3.53), that S_w^+ can be expressed in terms of S_w^- . Computations show, see Figure 8, that given any S_w^- there are two possible values for S_w^+ . However, in view of (3.31), we must restrict ourselves to the lower branch of Figure 8, which is a monotonically decreasing function of S_w^- . Note that S^* and S_* vary slightly with S_w^- . This dependence enters through u^+ .

As a result of (3.56) we find $S_g(\xi) = 0$ for all $\xi \geq 0$. Therefore we only need to consider the S_w -equation in problem P^r . Writing this equation as

$$\frac{dS_w}{d\xi} = F_w(S_w) = u^+ f_w^r(S_w) - vS_w - \{u^+ f_w^r(S_w^+) - vS_w^+\} \quad , \quad (3.57)$$

one easily verifies as a consequence of (3.31) and Figure 8 that $F_w(S_w) > 0$ for $S_w > S_w^+$ and $F_w(S_w) < 0$ for $S_w < S_w^+$. This implies that the only solution possible is

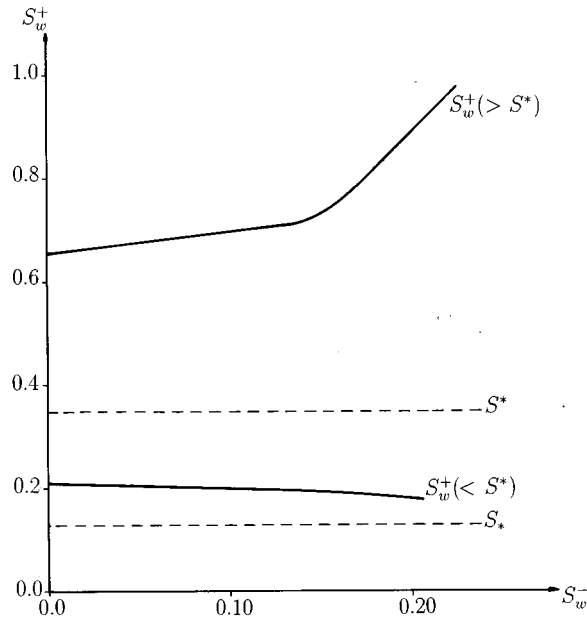


Figure 8: Possible saturation combinations (S_w^-, S_w^+) satisfying the Rankine-Hugoniot conditions (3.49) and condition (3.53).

$$S_w(\xi) = S_w^+ \quad \text{for all } \xi \geq 0 \quad . \quad (3.58)$$

Consequently $S_w^r = S_w^+$. Therefore the lower branch in Figure 8 also appears as $S_w^r(1)$ in Figure 7. By the monotonicity of the curves we find exactly one intersection point at $S_w^- = S_w^-(1)$. At this point the values of S_w^l and S_w^r are the same, implying a continuous water saturation in the transition model.

The corresponding values for S_g^-, S_w^+ and Λ are found from (3.53), Figure 7 and (3.49). The result is

$$S_w^- = 0.1240 \quad , S_g^- = 0.5339 \quad , S_w^+ = 0.2014 \quad , \Lambda = 0.9856 \quad , \quad (3.59)$$

implying that the steam condensation rate r is approximately equal to the steam injection rate u_{inj} . The S_w^+ -value is such that downstream the SCF the solution consists of a shock only. The composite solution as a path in the saturation-temperature space is shown as curve 1 in Figure 9. Note that the transition saturations are monotone functions of ξ : S_g is decreasing, while S_w is increasing. In Figure 10 we show the saturations as a function of $\eta = x/t$. This concludes the analysis of the base case.

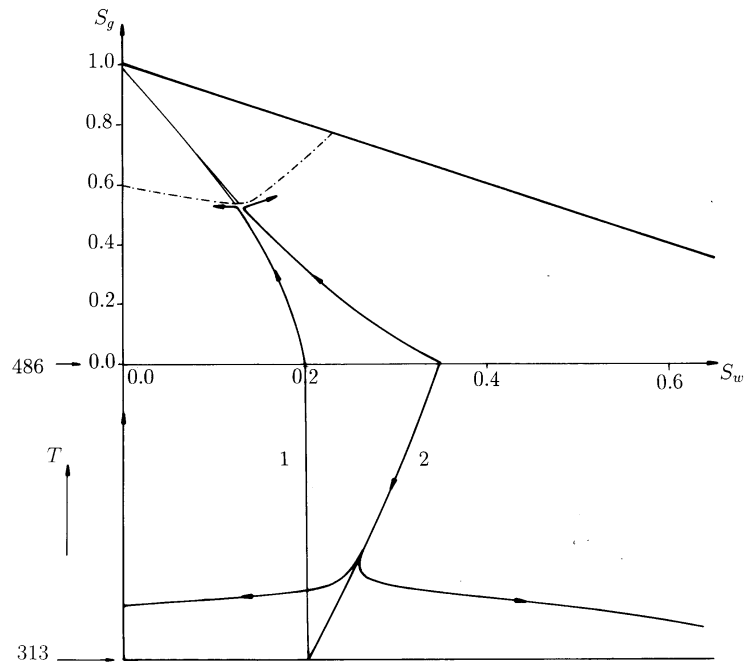


Figure 9: Composite solution as path in the phase-temperature space. Curve 1 reflects the base case, in which the transition temperature is piecewise constant. Curve 2 reflects the continuously varying temperature transition as given by (2.14). Here the orbits are pointing in the direction of the shooting procedures.

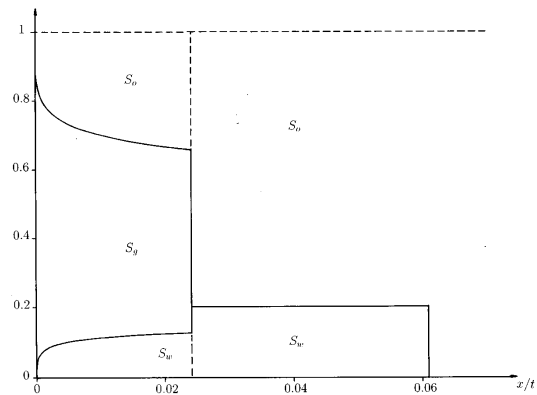


Figure 10: Saturation distribution as a function of $\eta = x/t$.

4 Nonuniqueness

In this section we investigate the relation between the transition model and the matching condition at the SCF in the global interface model. For this we use the three extensions of the base case, as introduced in Section 2.

4.1 Brooks-Corey capillary pressure diffusion

To incorporate the capillary pressure expressions (2.10) into the mathematical formulation of the base case, we start from Darcy's law for the individual phases

$$u_i = -k \frac{k_{ri}}{\mu_i} \frac{\partial p_i}{\partial x} \quad , \quad (4.1)$$

and use the definitions

$$P_c^{\text{ow}} = p_o - p_w \quad ; P_c^{\text{go}} = p_g - p_o \quad ; P_c^{\text{gw}} = p_g - p_w \quad , \quad (4.2)$$

to eliminate the pressures from the phase velocities. This gives

$$u_w = u f_w + f_w k \frac{k_{ro}}{\mu_o} \frac{\partial P_c^{\text{ow}}}{\partial x} + f_w k \frac{k_{rg}}{\mu_g} \frac{\partial P_c^{\text{gw}}}{\partial x} \quad (4.3)$$

$$u_o = u f_o - f_o k \frac{k_{rw}}{\mu_w} \frac{\partial P_c^{\text{ow}}}{\partial x} + f_o k \frac{k_{rg}}{\mu_g} \frac{\partial P_c^{\text{go}}}{\partial x} \quad (4.4)$$

$$u_g = u f_g - f_g k \frac{k_{ro}}{\mu_o} \frac{\partial P_c^{\text{go}}}{\partial x} - f_g k \frac{k_{rw}}{\mu_w} \frac{\partial P_c^{\text{gw}}}{\partial x} \quad (4.5)$$

where the total discharge u is given by (3.6) and the fractional flow functions f_i by (3.4), with power law relative permeabilities. Substituting these velocities into the phase balance equations and eliminating, as before, the oil saturation yields the modified transition equations for S_w and S_g . As in Section 3, we recast the equations in dimensionless form to obtain

$$\frac{\partial S_w}{\partial t} + \frac{\partial u f_w}{\partial x} = \frac{\rho_g}{\rho_w} \Lambda \delta(x - vt) - \varepsilon \frac{\partial}{\partial x} \left\{ f_w (k_{ro} + k_{rg} M_{og}) \frac{\partial J^{\text{ow}}}{\partial x} + f_w k_{rg} M_{og} \frac{\partial J^{\text{go}}}{\partial x} \right\} \quad (4.6)$$

$$\frac{\partial S_g}{\partial t} + \frac{\partial u f_g}{\partial x} = -\Lambda \delta(x - vt) + \varepsilon \frac{\partial}{\partial x} \left\{ f_g (k_{ro} + k_{rw} M_{ow}) \frac{\partial J^{\text{go}}}{\partial x} + f_g k_{rw} M_{ow} \frac{\partial J^{\text{ow}}}{\partial x} \right\} \quad (4.7)$$

where we have used $P_c^{\text{gw}} = P_c^{\text{go}} + P_c^{\text{ow}}$ and expressions 2.10 for P_c^{go} and P_c^{ow} . The Leverett functions follow from (2.10) and (2.12) and the dimensionless number ε results from (3.36) and (2.13):

$$\varepsilon = \frac{D}{u_{\text{inj}}L} = \frac{\sigma\sqrt{\phi k}}{\mu_o u_{\text{inj}}L} . \quad (4.8)$$

Note that ε is related to the capillary number (capillary forces / viscous forces). Since we have assumed that $J^{\text{ow}} = J^{\text{ow}}(S_w)$ and $J^{\text{og}} = J^{\text{og}}(S_g)$, we give equations (4.7) and (4.7) the more convenient form

$$\frac{\partial S_w}{\partial t} + \frac{\partial u f_w}{\partial x} = \frac{\rho_g}{\rho_w} \Lambda \delta(x - vt) + \varepsilon \frac{\partial}{\partial x} \left\{ D_{\text{ww}} \frac{\partial S_w}{\partial x} + D_{\text{wg}} \frac{\partial S_g}{\partial x} \right\} \quad (4.9)$$

$$\frac{\partial S_g}{\partial t} + \frac{\partial u f_g}{\partial x} = -\Lambda \delta(x - vt) + \varepsilon \frac{\partial}{\partial x} \left\{ D_{\text{gw}} \frac{\partial S_w}{\partial x} + D_{\text{gg}} \frac{\partial S_g}{\partial x} \right\} \quad (4.10)$$

These equations replace the base case equations (3.37) and (3.38). We now proceed as in Section (3.2). That is we introduce the scaled travelling wave coordinate ξ in equations (4.10) and (4.10) and assume travelling wave type profiles for the solutions. Integrating the resulting ordinary differential equations and applying boundary conditions (3.47), (3.48) yields the same Rankine Hugoniot conditions as before. Instead of subproblems P^l and P^r , we now obtain for $\xi < 0$

$$Q^l \left\{ \begin{array}{l} D_{\text{ww}}^l \frac{dS_w}{d\xi} + D_{\text{wg}}^l \frac{dS_g}{d\xi} = f_w^l - v S_w - (f_w^- - v S_w^-) \\ D_{\text{gw}}^l \frac{dS_w}{d\xi} + D_{\text{gg}}^l \frac{dS_g}{d\xi} = f_g^l - v S_g - (f_g^- - v S_g^-) \\ S_w(-\infty) = S_w^- , S_w(0) = S_w^l \\ S_g(-\infty) = S_g^- , S_g(0) = 0 \quad , \end{array} \right. \quad (4.11)$$

and for $\xi > 0$

$$Q^r \left\{ \begin{array}{l} D_{\text{ww}}^r \frac{dS_w}{d\xi} + D_{\text{wg}}^r \frac{dS_g}{d\xi} = u^+ f_w^r - v S_w - (u^+ f_w^+ - v S_w^+) \\ D_{\text{gw}}^r \frac{dS_w}{d\xi} + D_{\text{gg}}^r \frac{dS_g}{d\xi} = u^+ f_g^r - v S_g \\ S_w(+\infty) = S_w^+ , S_w(0) = S_w^r \\ S_g(+\infty) = 0 , S_g(0) = 0 \quad , \end{array} \right. \quad (4.12)$$

where we have used condition (3.56). The upper indices in the diffusion coefficients relate to the temperature difference across the SCF. The properties of the nonlinear functions imply (for $j = l, r$)

$$D_{ww}^j, D_{gg}^j > 0 \quad \text{and} \quad D_{wg}^j, D_{gw}^j < 0 \quad . \quad (4.13)$$

and

$$D_{ww}^j D_{gg}^j > D_{wg}^j D_{gw}^j \quad (4.14)$$

in \mathcal{D} . Because we are modifying only the transition model, conditions (3.26) and (3.31) remain unchanged.

We first consider the solvability of Problem Q^l . As in the base case the behavior of solutions depends critically on the location of the equilibrium point (S_w^-, S_g^-) . Inequalities (4.13) and (4.14) imply that the diffusion matrix is positive definite. This means that the number and location of equilibrium points in Problems Q^l and P^l are identical. Of course the curves where $dS_w/d\xi = 0$ and $dS_g/d\xi = 0$ are different. Two typical cases are shown in Figure 11, where we introduced again the variable $\zeta = -\xi$ (i.e. we computed orbits in the positive ζ direction).

As in the base case, equilibrium points $(S_w^-, S_g^-) \in \mathcal{D}_l$ (bottom figure) cannot be reached. What remains is again the possibility $(S_w^-, S_g^-) \in l$. Selecting points on the curve l , corresponding initial points S_w^l were found numerically yielding a dependence which closely resembles the one shown in Figure 7. Observe from Figure 11 that now the water saturation in the transition region is not monotone: in the direction of negative ξ it first increases, reaches a global maximum and then decreases towards S_w^- at $\xi = -\infty$.

We established computationally that solutions of Problem Q^r satisfy $dS_g/d\zeta > 0$ for S_g close to zero. Together with the boundary conditions this implies $S_g(\xi) = 0$ for all $\xi \geq 0$. A similar argument as in Section 3.3 gives here again $S_w(\xi) = S_w^+$ for all $\xi \geq 0$. We then apply the procedure outlined in Section 3.2 and find for different values of the sorting factor λ_s , different interface saturations. Corresponding to $\lambda_s = 2$ we established:

$$S_w^- = 0.1452 \quad , S_g^- = 0.5467 \quad , S_w^+ = 0.1990 \quad , \Lambda = 0.9855 \quad . \quad (4.15)$$

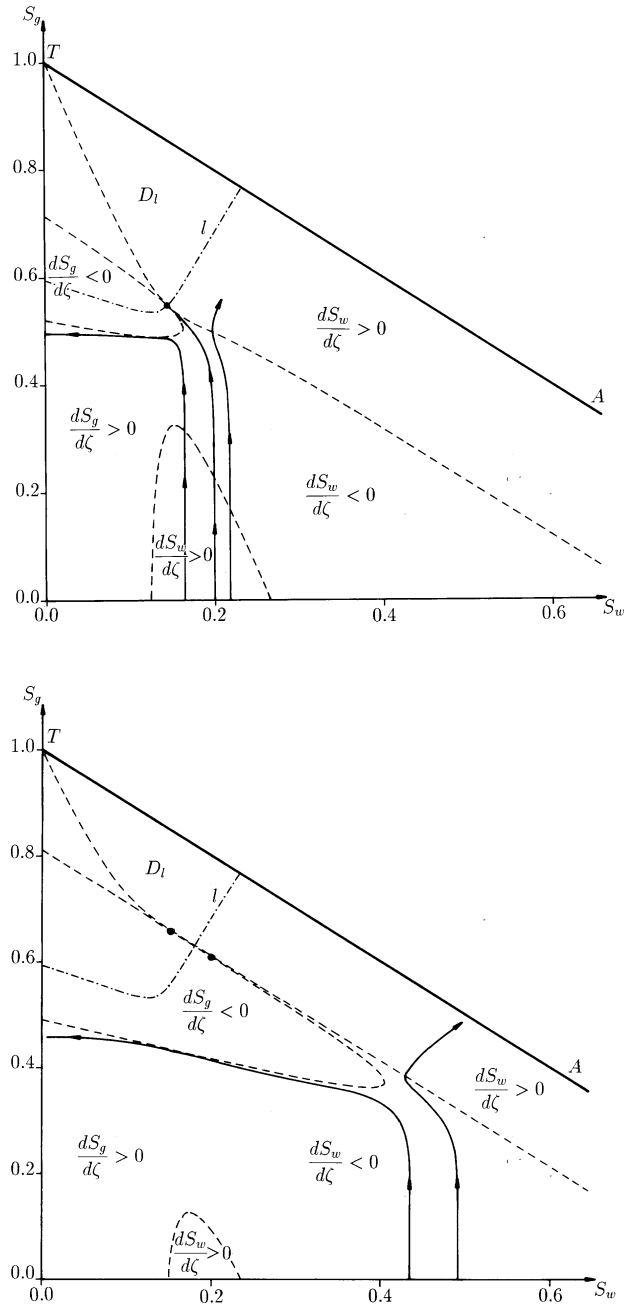


Figure 11: Shooting procedure to solve Problem Q^1 . Here $S_g(0) = 0$ Top: flow diagram for $(S_w^-, S_g^-) \in l$. Bottom: flow diagram for $(S_w^-, S_g^-) \in \mathcal{D}_l$. The dots indicate the location of equilibrium points. Again $\zeta = -\xi$.

4.2 Temperature variation

Next we modify the temperature distribution in the transition model. Instead of the discontinuous temperature (2.8), we will now investigate the consequence of the continuous expression (2.14). Clearly this modification leaves the transition model for $\xi < 0$ unchanged. In particular conditions (3.53) and (3.31), the Rankine Hugoniot conditions (3.49) and the results for problem P^l , with $S_g(0) = 0$, are the same as in the base case. Thus with reference to Figure 7, we use the same S_w^l curve.

The only change occurs in Problem P^r where now the temperature variation with ξ enters in the fractional flow functions ($f_i^r = f_i(S_w, S_g, T(\xi))$) through the mobility ratios. This dependence has no consequence for the steam saturation downstream the SCF. Since $u^+ f_g - v S_g < 0$ for small values of S_g , the only possible solution satisfying the S_g - equation and boundary conditions is $S_g(\xi) = 0$ for all $\xi \geq 0$. What remains to be considered is the S_w - equation.

$$\frac{dS_w}{d\xi} = u^+ f_w(S_w, T(\xi)) - v S_w - (u^+ f_w^+ - v S_w^+) \quad (4.16)$$

for $\xi > 0$. Using the exponential relation in (2.14), we write this equation with the temperature as independent variable

$$\frac{dS_w}{dT} = \frac{u^+ f_w(S_w, T) - v S_w - (u^+ f_w^+ - v S_w^+)}{-\alpha(T - T_o)} \quad (4.17)$$

with $T_o < T < T_1$. The corresponding boundary conditions are

$$S_w(T_o) = S_w^+ \quad \text{and} \quad S_w(T_1) = S_w^r \quad . \quad (4.18)$$

Because (T_o, S_w^+) is a singular point of equation (4.17), we solve it backwards in T. Thus given a value for S_w^+ , we start at $T = T_1$ and use the iterative shooting method again to obtain an accurate approximation of the corresponding values for S_w^r .

In particular we find for any given S_w^- , which yields a unique S_w^+ from Figure 8, a unique water saturation at the right side of the SCF. This saturation, which is denoted by $S_w^r(2)$ in Figure 7, depends also monotonically on S_w^- . Consequently there is again exactly one intersection point at $S_w^- = S_w^-(2)$. As before the values for S_g^-, S_w^+ and Λ are found from (3.53), Figure 7 and (3.49):

$$S_w^-(2) = 0.1288 \quad , S_g^- = 0.5337 \quad , S_w^+ = 0.2010 \quad , \Lambda = 0.9856 \quad , \quad (4.19)$$

The composite solution as a path in the saturation-temperature space is shown as curve 2 in Figure 9. Note the significant change in the transition region, in particular the striking non-monotonicity of S_w , but the minor change in the hyperbolic part of the path, i.e. the outer solution.

4.3 Positive steam saturation at SCF

Finally we modify the base case by replacing condition (3.56). Now we assign a positive value $S_g(0)$ to the steam saturation at the SCF. This does not involve conditions (3.53), (3.31) and (3.49), which therefore remain unchanged here. To find the saturations in the transition region, we now have to solve subproblems P^l and P^r subject to $S_g^l = S_g^r = S_g(0) > 0$. With reference to Figure 12, we apply iterative shooting procedures, starting from the line $S_g = S_g(0)$: Problem P^l is solved backwards in ξ (or as before, in positive $\zeta = -\xi$ direction) and Problem P^r is solved forwards in ξ .

Given S_w^- , we first determine S_w^+ from Figure 8 and then solve Problems P^l and P^r repeatedly to obtain accurate approximations for S_w^l and S_w^r . Again this leads to two monotone curves: S_w^l is increasing and S_w^r is decreasing with respect to S_w^- . The unique intersection point gives the required value for S_w^- . The saturations S_g^- and S_w^+ , and the condensation rate Λ follow as before. Corresponding to $S_g(0) = 0.035$, the result is

$$S_w^-(2) = 0.1237 \quad , S_g^- = 0.5339 \quad , S_w^+ = 0.2015 \quad , \Lambda = 0.9856 \quad . \quad (4.20)$$

We have tried to take larger values of $S_g(0)$, but were not able to carry out the construction. In particular Problem P^r appears very sensitive with respect to the choice of $S_g(0)$.

5 Practical Aspects

Practical aspects of the one dimensional steamdrive model presented here concern: prediction of remaining oil in tube experiments, comparison for validation of simulators, and investigation of effect of parameter variations. In many field cases the remaining oil in the steam zone can be modelled as a gravity drainage process. Our model deals with the opposite case

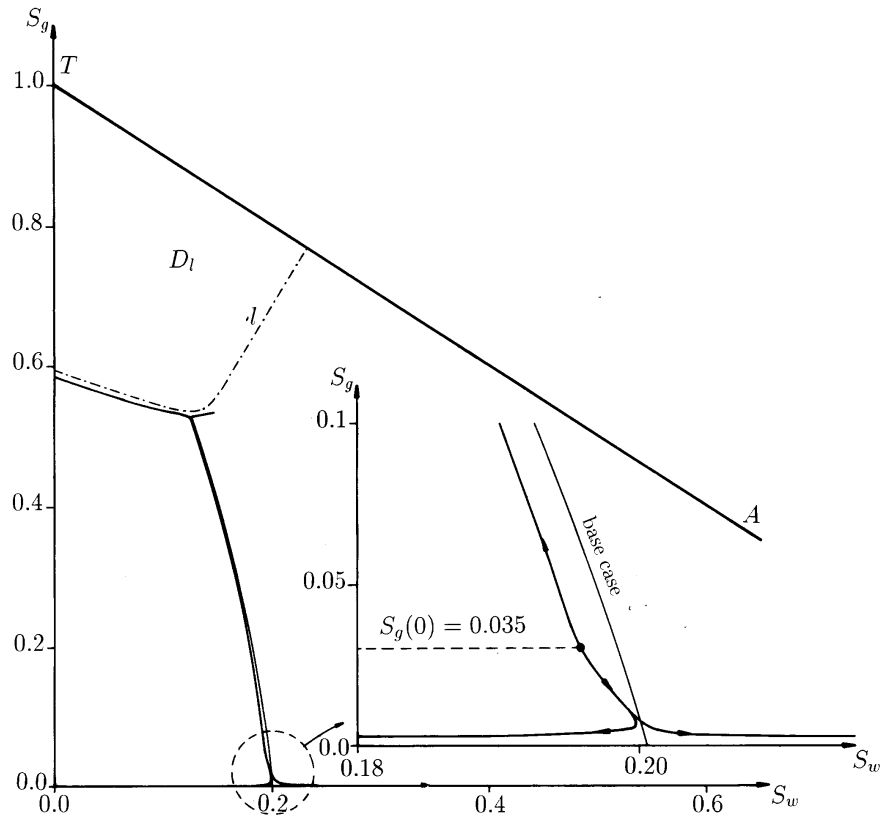


Figure 12: Orbits in the saturation space, starting with a positive value of the steam saturation at the SCF, $S_g(0) > 0$.

when the flow of each of the phases occurs along the same stream lines, i.e. in the absence of gravity segregation effects across stream lines. Actually the work described here started as an attempt to interpret vertical steam flood experiments. Also our model does not deal explicitly with heat losses. The purpose of this section is, however, to show the practical relevance of the analysis described above. In other words, we want to show that the detailed modelling of the condensation process in the transition zone (in the limit of zero length) is required for accurate interpretations. The average oil saturation remaining in the steam zone is of interest in all of these applications. We use Figure 13 to illustrate both the influence of the transition model on the global steam displacement process and the dependence of the displacement efficiency on a number of parameters (e.g. the oil viscosity). Before we do this we make a few practical remarks.

Oil recovery from the steam swept zone is high due to two mechanisms: film flow of oil and distillation of volatile components. For heavy oil the distillation effect is usually of minor importance, see for instance Bruining et al. [2]. Film flow of oil can occur when oil spreads on water in the presence of steam. Film flow can be modelled by non-zero relative permeabilities at low oil saturation, and is thus contained in the model. Here we use zero residual oil saturations to describe film flow.

All examples discussed in this paper use 100 % steam injection quality. It can be shown, however, that lower steam qualities have no effect on the average oil saturation in the steam zone. This observation follows from the properties that the saturations (S_w^-, S_g^-, S_o^-) do not depend on the boundary condition for practically occurring steam qualities, and that the average oil saturation in the steam zone only depends on (S_w^-, S_g^-, S_o^-) .

The first property is explained as follows. When steam of less than 100 % quality is injected, the solution path in Figure 4 does not start at the apex but on one of the slow paths leaving the line $S_o = S_{or} = 0$. The starting position on the line $S_o = S_{or} = 0$ is determined by the volume fraction of liquid water (with respect to the total volume of water and steam). Due to the density difference between steam and water this point will be close to the apex for all situations of practical interest. At the line $S_o = S_{or} = 0$ the smallest eigenvalue is zero and hence the solution starts as a slow rarefaction. Subsequently the solution path "jumps" on the same fast path as we would have obtained with 100 % steam quality. As a result we obtain a solution which first is a slow rarefaction, followed by a constant state, and then a fast rarefaction until the solution reaches the curve ℓ where (3.53) holds. From there the solution follows from the same procedure which we used for the 100 % steam quality injection case. Hence we obtain the same values of (S_w^-, S_g^-, S_o^-) just upstream of the SCF.

The second property follows from the fact that the average oil saturation in the steam

zone, \bar{S}_o , can be expressed in terms of the saturation S_o^- and the fractional flow function f_o^- just upstream of the SCF, irrespective of the saturation distribution within the zone. In fact it can be shown that ²

$$\bar{S}_o = S_o^- - \frac{u}{v} f_o^- \quad (5.1)$$

where the dimensionless velocity $u=1$. The same result for two-phase flow problems can be found in standard reservoir engineering textbooks, for instance Dake [3] and Dullien [4].

In Figure 13 we plot \bar{S}_o , obtained with the procedure described in Sections 3 and 4, against the average oil saturation \bar{S}_o^{\min} , which is obtained from a simple approximation. This approximation assumes that the oil saturation just upstream of the SCF can be approximated by the oil saturation that satisfies equation (3.53) for the minimum possible steam saturation. It turns out to be useful for crude estimates and showing trends, but not for accurate interpretations.

For all cases we only vary one parameter with respect to the base case given in Table I. In all computations we use three-phase relative permeabilities. The three-phase permeabilities are obtained by the combination of Brooks-Corey two-phase relative permeabilities and the modified Stones I method, see Fayers & Matthews [6]. In the expressions we take $S_{or} = 0$. We give the relations in full dimensional form:

$$\begin{aligned} k_{rw} &= k'_{rw} S_{we}^{\frac{2+3\lambda_s}{\lambda_s}} \\ k_{rg} &= k'_{rg} (1 - S_{ge})^2 (1 - S_{ge}^{\frac{2+\lambda_s}{\lambda_s}}) \\ k_{ro} &= \frac{S_o(1 - S_{wc})}{k_{rcow}(1 - S_w)(1 - S_{wc} - S_g)} k_{row} k_{rog} \end{aligned}$$

where

$$S_{we} = \frac{S_w - S_{wc}}{1 - S_{wc}}, \quad S_{ge} = \frac{1 - S_g - S_{wc}}{1 - S_{wc}}$$

and

$$k_{row} = k'_{rg} (1 - S_{we})^2 (1 - S_{we}^{\frac{2+\lambda_s}{\lambda_s}}), \quad k_{rog} = k'_{rw} S_{ge}^{\frac{2+3\lambda_s}{\lambda_s}}.$$

We use for the end-point permeability of the wetting phase at residual non-wetting phase saturation $k'_{rw}=0.5$ and for the end-point permeability of the non-wetting phase at connate wetting phase saturation $k'_{rg}=1.0$. Finally we use $k_{rcow} = 1$. To emphasize the effect of film

²In full dimensional form $\bar{S}_o = S_o^- - u_{inj} f_o^- / (v_{st} \phi)$

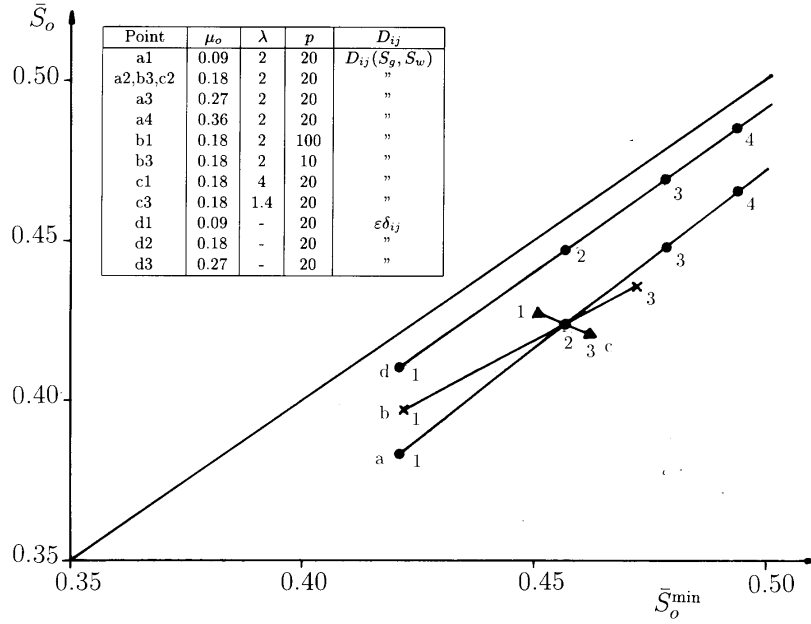


Figure 13: Comparison of average oil saturation calculated from full computations and calculated with the "approximate minimum condition"

flow, the expression for k_{row} and k_{rog} are different from the ones proposed by Fayers and Matthews.

In line d in Figure 13 we vary the cold oil viscosity in the medium viscosity range, i.e. between 0.09-0.27 [Pa s]. Moreover we use saturation independent capillary diffusion. We observe that the result is close to the $\bar{S}_o = \bar{S}_o^{\min}$ line, implying that for this case the approximative method is of good quality. As can be expected, an increasing oil viscosity leads to a deteriorating displacement efficiency with an increasing oil saturation in the steam zone. In all other cases we use saturation dependent capillary diffusion. In line a we vary again the viscosity as in line d. However, line a and line d are significantly different only due to the fact that we use different capillary pressure behavior in the transition zone. In line c we vary the sorting factor λ_s and this affects both the relative permeabilities and the capillary diffusion. We observe that the deviation from the $\bar{S}_o = \bar{S}_o^{\min}$ line depends on λ_s . For reasons of practical interest we also show the effect of pressure variation. The steam pressure is not explicit in our equations but affects a number of parameters given in Table I. We use empirical relations given in Tortike & Farouq Ali [24] to represent the steam tables. First the pressure determines the (boiling) temperature. It also has a small effect on the enthalpy for the conversion of cold water to hot steam (ΔH). Therefore the steam condensation front velocity decreases at higher pressures, see (2.4). Secondly a high pressure, through its influence on temperature, enhances

the steam viscosity and lowers the liquid viscosities. Direct pressure effects on viscosities are negligible. The pressure range is between 10 and 100 bar. Indeed the displacement efficiency improves with increasing pressure. We note that this occurs at the expense of a much higher mass of injected steam per unit volume of recovered oil, because higher temperatures are involved now; the reservoir must be heated to a higher temperature.

We end with a remark bearing on numerical simulation. If Brooks-Corey capillary diffusion is explicitly taken into account in the physical model, the water saturation profile may show a peak due to the non-monotone nature of the water saturation profile in the transition zone, see Figure 11.

6 Conclusions

Based on the results of this paper we conclude the following:

- A hyperbolic model for oil recovery by steamdrive requires a parabolic transition sub-model to obtain unique results.
- Model results depend on details of the transition submodel, even in the limit of zero transition length.
- As a consequence no universal entropy condition can be formulated which guarantees uniqueness for the hyperbolic limit problem.
- The effect of the rate of temperature decline and the effect of presence of steam downstream the Steam Condensation Front is small.
- The effect of Brooks-Corey capillary diffusion instead of constant (saturation independent) capillary diffusion is well noticeable.
- An approximate solution is given, based on the minimum of the l -curve in domain \mathcal{D} . The validity of this approximation can be checked from Figure 13 for different values of the model parameters.

References

- [1] Aziz, K. and Settari, A., *Petroleum Reservoir Simulation*, Applied Science Publishers, London (1979).

- [2] Bruining, J., Batenburg, D.W. van, De Haan, H.J., Quak, R. and Palmgren, C.T.S., *The efficiency of the distillation mechanisms to enhance steamdrive recovery*. In: Proc. of the 4th Symposium on Enhanced Oil Recovery, Hamburg (October-1987).
- [3] Dake, L.P., *Fundamentals of Reservoir Engineering*, Elsevier Science Publishers, Amsterdam (1978).
- [4] Dullien, F.A.L., *Porous Media; Fluid Transport and Pore Structure*, Academic Press, N.Y. (1979).
- [5] Farouq Ali, S.M., Doan, Q, Matthias, R.C.M. and George, A.E., *Study of steamflood performance in stratified reservoirs*. In: Proc. of the 45th Annual Technical Meeting of the Petroleum Society of CIM, Calgary (June-1994).
- [6] Fayers, F.J. and Matthews, J.D., *Evaluation of Normalized Stone's Methods for Estimating Three-Phase Relative Permeabilities*, Soc. Pet. Eng. J., (1984) 224-232.
- [7] Godderij, R.R.G.G., Bruining, J. and Molenaar, J., *A Fast 3D Interface Simulator for Steam Drives*, SPE-Western Regional Meeting (June-1997) 279-289 (SPE-38288).
- [8] Gümrah, Palmgren, C.T.S., Bruining, J. and Godderij, R.R.G.G., *Steamdrive in a layered reservoir: an experimental and theoretical study*. In: Proc. SPE/DOE 8th Symposium on Enhanced Oil Recovery, Tulsa (April-1992), 159-167 (SPE/DOE 24171).
- [9] Hellferich, F.G., *Theory of multicomponent, multiphase displacement in porous media*, Soc. Pet. Eng. J., **271** (1981) 51-74.
- [10] Kimber, K.D., Farouq Ali, S.M., and Puttagunta, V.R., *New scaling criteria and their relative merits for steam recovery experiments*, J. Cdn. Pet. Tech., **27** (1988) 86-94.
- [11] Lax, P., *The Formation and Decay of Shock Waves*, Amer. Math. Monthly, **79** (1972) 227-241.
- [12] LeVeque, R.J., *Numerical Methods for Conservation Laws*, Birkhäuser Verlag, Basel (1992).
- [13] Liu, T.P. *Uniqueness of weak solutions of the Cauchy problem for general 2x2 conservation laws*, Journal of Differential Equations **20** (1976) 369-388.
- [14] Mandl, G., and Volek, C.W., *Heat and mass transport in steamdrive processes*, Soc. Pet. Eng. J., (1969) 57-79.

- [15] Menegus, D.K. and Udell, K.S., *A study of steam injection into water saturated capillary porous media*, SPE Reservoir Engineering (1988).
- [16] Miller, C.A., *Stability of moving surfaces in fluid systems with heat and mass transport, III. Stability of displacement fronts in porous media*, AIChE Journal **21** (1975) 474-479.
- [17] Pope, G.A., *The application of fractional flow theory to enhanced oil recovery*, Soc. Pet. Eng. J., **20** (1980) 191-205.
- [18] Prats, M., *Thermal Recovery*, SPE Henry L. Doherty Series, Monograph 7, Dallas (1982).
- [19] Reid, R.C., Prausnitz, J.M., and Sherwood, T.K., *The Properties of Gases and Liquids*, McGraw-Hill, N.Y. (1977).
- [20] Schaeffer, D.G. and Shearer, M, *The classification of 2x2 systems of non- strictly hyperbolic conservation laws, with application to oil recovery*, Commun. Pure Appl. Math., **40** (1987) 141-178.
- [21] Shutler, N.D., *A one dimensional analytical technique for predicting oil recovery by steam flooding*, Soc. Pet. Eng. J., (1972) 489-498.
- [22] Smoller, J., *Shock Waves and Reaction-Diffusion Equations*, Springer-Verlag, New York (1980).
- [23] Stewart, L.D. and Udell, K.S., *Mechanisms of residual oil displacement by steam injection*, SPE Reservoir Engineering, (November-1988) 1233-1242.
- [24] Tortike, W.S. and Farouq Ali, S.M.: *Saturated-steam-property functional correlations for fully implicit thermal reservoir simulation*, SPE Reservoir Engineering, (November-1989) 471-474.
- [25] Udell, K.S., *The thermodynamics of evaporation and condensation in porous media*, California Regional Meeting of the Society of Petroleum Engineers, San Francisco, (March-1982) (SPE 10779).
- [26] Udell, K.S., and Fitch, J.S., *Heat and mass transfer in capillary porous media considering evaporation, condensation and non-condensable gas effects*,
- [27] Wingard, J.S. and Orr, F.M., *An analytical solution for steam/oil/water displacements*, SPE Advanced Technology Series, **2** (1994) 167-176.

- [28] Yortsos, Y.C., *Distribution of fluid phases within the steam zone in steam injection processes*, Soc. Pet. Eng. J., (1984) 458-466.